

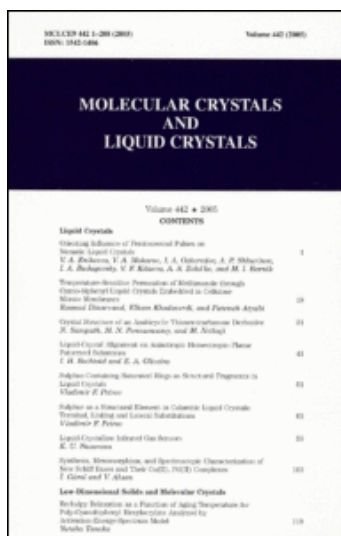
This article was downloaded by:

On: 20 January 2011

Access details: *Access Details: Free Access*

Publisher *Taylor & Francis*

Informa Ltd Registered in England and Wales Registered Number: 1072954 Registered office: Mortimer House, 37-41 Mortimer Street, London W1T 3JH, UK



MOLECULAR CRYSTALS AND LIQUID CRYSTALS	
Volume 442 • 2005	
CONTENTS	
Liquid Crystals	
Viscosity Behavior of Hexamethyl Polysiloxane in Various Liquid Crystals	1
V. A. Podinovskii, V. A. Malozemov, I. A. Gilyarov, A. P. Shibaev, I. A. Rudakovskii, V. P. Kabanov, A. A. Zakharenko, and M. I. Berezin	
Temperature-Induced Permeation of Polystyrene through Crosslinked Liquid Crystals Embedded in Cellulose Matrix Membranes	10
Ramona Dinculescu, Elvira Khatunova, and Patrick Arault	
Crystal Structure of an Anisotropic Thermotropic Liquid Crystalline Polymer	21
A. S. Berezin, M. N. Potomarenko, and M. Jurek	
Liquid Crystal Alignment on Anisotropic Hexamethyl Polysiloxane	41
J. H. Bredas and C. A. Ollivier	
Substrate Containing Hexamethyl Polysiloxane and Tripropyl in Liquid Crystals	51
Yoshihiro H. Fukuoka	
Substrate as a Structural Element in Columnar Liquid Crystals: Thermal Stability and General Substitutions	61
Yoshihiro H. Fukuoka	
Liquid Crystals: Infrared Gas Sensors	81
M. T. Hsueh	
Optical, Microscopic, and Spectroscopic Characterization of New 9-BB Dyes and Their Gels, PHEC Composites	101
J. Chen and Y. Shen	
Low Dimensional Solids and Molecular Crystals	
Refractive Birefringence as a Function of Aging Temperature for Polydimethylsiloxane Membranes: Analysis by Infrared Spectroscopy, X-ray	119
Michiko Tamaki	

Molecular Crystals and Liquid Crystals

Publication details, including instructions for authors and subscription information:

<http://www.informaworld.com/smpp/title~content=t713644168>

X-ray, Dielectric and High Pressure Studies on a Compound Exhibiting Ferro-, Ferri- and Antiferroelectric Smectic Phases

D. Shankar Rao^a; S. Krishna Prasad^a; S. Chandrasekhar^a; S. Mery^b; R. Shashidhar^c

^a Centre for Liquid Crystal Research, Bangalore, India ^b Institut de Physique et chimie de Materiaux de Strasbourg, Strasbourg, France ^c Naval Research Laboratory, Centre for Bio/Molecular Science & Engg., Washington, DC, USA

First published on: 01 January 1997

To cite this Article Rao, D. Shankar , Prasad, S. Krishna , Chandrasekhar, S. , Mery, S. and Shashidhar, R.(1997) 'X-ray, Dielectric and High Pressure Studies on a Compound Exhibiting Ferro-, Ferri- and Antiferroelectric Smectic Phases', *Molecular Crystals and Liquid Crystals*, 292: 1, 301 – 310

To link to this Article: DOI: 10.1080/10587259708031939

URL: <http://dx.doi.org/10.1080/10587259708031939>

PLEASE SCROLL DOWN FOR ARTICLE

Full terms and conditions of use: <http://www.informaworld.com/terms-and-conditions-of-access.pdf>

This article may be used for research, teaching and private study purposes. Any substantial or systematic reproduction, re-distribution, re-selling, loan or sub-licensing, systematic supply or distribution in any form to anyone is expressly forbidden.

The publisher does not give any warranty express or implied or make any representation that the contents will be complete or accurate or up to date. The accuracy of any instructions, formulae and drug doses should be independently verified with primary sources. The publisher shall not be liable for any loss, actions, claims, proceedings, demand or costs or damages whatsoever or howsoever caused arising directly or indirectly in connection with or arising out of the use of this material.

X-ray, Dielectric and High Pressure Studies on a Compound Exhibiting Ferro-, Ferri- and Antiferroelectric Smectic Phases

D. S. SHANKAR RAO^a, S. KRISHNA PRASAD^a,
S. CHANDRASEKHAR^{a,*}, S. MERY^b and R. SHASHIDHAR^c

^aCentre for Liquid Crystal Research, Jalahalli, Bangalore 560 013, India;

^bInstitut de Physique et chimie de Materiaux de Strasbourg, G.M.O.,
23 rue du Loess, 67037 Strasbourg, France;

^cNaval Research Laboratory, Centre for Bio/Molecular Science & Engg.,
4555 Overlook Avenue SW, Washington DC 20375-5348, USA

We report X-ray layer spacing, dielectric constant and high pressure measurements on a compound that exhibits the following sequence of phase transitions: smectic A-ferroelectric smectic C*-ferrielectric smectic C_γ*-antiferroelectric smectic C_λ*-hexatic antiferroelectric smectic I_A*-crystal K. The pressure-temperature diagram shows two *three-phase* meeting points, which are topologically consistent with critical end points, and reentrant behavior of the C* and C_γ* phases as the pressure is varied at *constant* temperature.

Keywords: Ferroelectric; ferrielectric; antiferroelectric; smectics; X-ray; dielectric constant; high pressure studies; pressure temperature phase diagram; critical end point

INTRODUCTION

Studies on materials exhibiting the antiferroelectric and ferrielectric smectic phases have gained considerable importance in recent years [1]. In this paper we report X-ray, dielectric and high pressure studies on a new compound showing smectic A-ferroelectric smectic C*-ferrielectric smectic C_γ*-antiferroelectric smectic C_λ*-hexatic antiferroelectric smectic I_A* phase

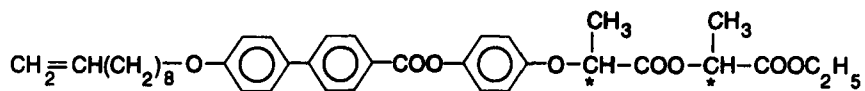
*Corresponding author.

Phone: 91 80 838 2924; Fax: 91 80 838 2044.

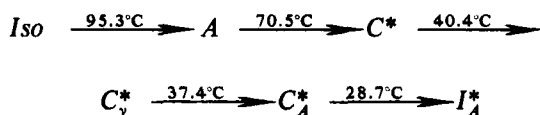
sequence. We also present new results on the effect of pressure on the $C^* - C_\gamma^*$, $C_\gamma^* - C_A^*$ and $C_A^* - I_A^*$ phase boundaries.

EXPERIMENTAL

Experiments have been conducted on 1-(R)-[1-(S)(ethyloxy carbonyl) ethoxy carbonyl] ethyloxycarbonyl 4'-(9-decenyloxy) biphenyl-4-carboxylate. The structural formula and the transition temperatures (as obtained by DSC) for this compound are given below, while the details regarding its synthesis will be reported elsewhere.



(R, S)



The optical textural changes across $C^* - C_\gamma^*$ and $C_\gamma^* - C_A^*$ transitions were closely similar to the ones described by Faye *et al.* [2]. The texture of the I_A^* phase was also seen to resemble the standard texture for smectic I described in the literature. With these observations, together with the X-ray and dielectric studies to be presented below, all the phases could be identified unambiguously.

For X-ray layer spacing measurements, a computer controlled diffractometer (Huber 644) was used [3]. The sample contained in a sealed Lindemann glass capillary of 0.5 mm diameter was aligned by cooling from the isotropic phase in the presence of a magnetic field. The layer spacing in the I_A^* phase could not be determined because the sample invariably crystallised just before $C_A^* - I_A^*$ transition.

Dielectric measurements were made on 50 μm thick samples contained in ITO coated glass cells treated with polyimide solution and rubbed. However, with 50 μm thick samples, measurements were not possible in the I_A^* phase because the material crystallised in the C_A^* phase just before the $C_A^* - I_A^*$ transition. With 9 μm samples, on the other hand, crystallisation did not take place and measurements on the I_A^* phase were possible. The temperature was controlled by a hot stage-processor combination (Mettler

FP82-FP90). To improve the precision in measuring the sample temperature, a calibrated bead thermistor (YSI 44011) was located very close to the sample. The thermistor output was read on a digital multimeter (HP 34401A). The frequency, temperature and bias field dependence of the dielectric constant was measured using an impedance analyser (HP 4194A). The multimeter, the impedance analyser and the Mettler processor were interfaced to a PC for data acquisition and control.

High pressure studies were carried out using an optical cell with the sample sandwiched between sapphire windows and isolated from the pressure transmitting fluid by an elastomer tube. The transition temperatures were determined by the optical transmission technique (For details of this set-up see Ref. 4). In contrast to what happens at atmospheric pressure, the I_A^* phase supercooled appreciably at elevated pressures.

RESULTS AND DISCUSSION

Figure 1 shows the layer spacing d as a function of temperature in the A , C^* , C_γ^* and C_A^* phases. At the $A - C^*$ transition, there is an abrupt change in the slope of d vs. temperature but as there is no discontinuity in the value of d , nor a two-phase coexistence region, the transition may be taken to be of second order. At the $C^* - C_\gamma^*$ and $C_\gamma^* - C_A^*$ transitions neither the

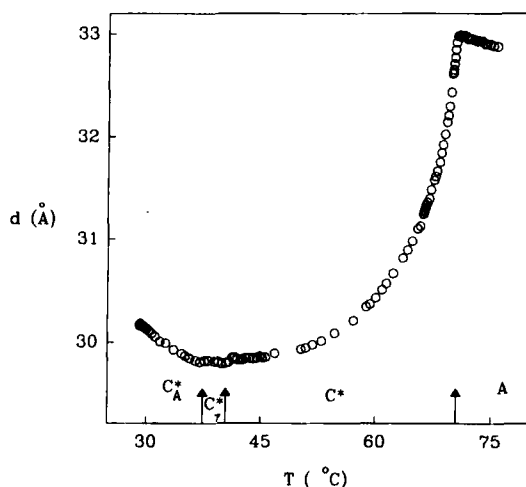


FIGURE 1 Temperature dependence of the layer spacing. The arrows indicate the transition temperatures determined by DSC. Owing to the crystallisation of the sample, no data could be obtained in the I_A^* phase.

magnitude of d nor its slope hardly change. These features are in agreement with earlier observations [5]. In the C_A^* phase, just below the $C_\gamma^* - C_A^*$ transition, d reverses its trend and starts increasing with decreasing temperature. This increase can be interpreted as due to the occurrence of the hexatic I_A^* phase below C_A^* . However, as mentioned earlier, X-ray measurements in I_A^* phase could not be carried out because of the crystallisation of the sample. The variation of d in the C_A^* phase is very similar to that reported recently by Neundorf *et al.* [6] in a mixture of MHPOBC/MHO BMB, which also shows $C_A^* - I_A^*$ transition.

The thermal variation of the dielectric constant ϵ' at different frequencies is plotted in Figure 2a. Near the $A - C^*$ transition, there is a rapid increase in the value of ϵ' , the magnitude of which decreases as the frequency is increased. The features are explainable in terms of the contribution due to the two relaxation modes, viz., the Goldstone mode and the soft mode. As the temperature is lowered, around 40°C there is a large drop in ϵ' values at low frequencies and a small increase in the value for the high frequency

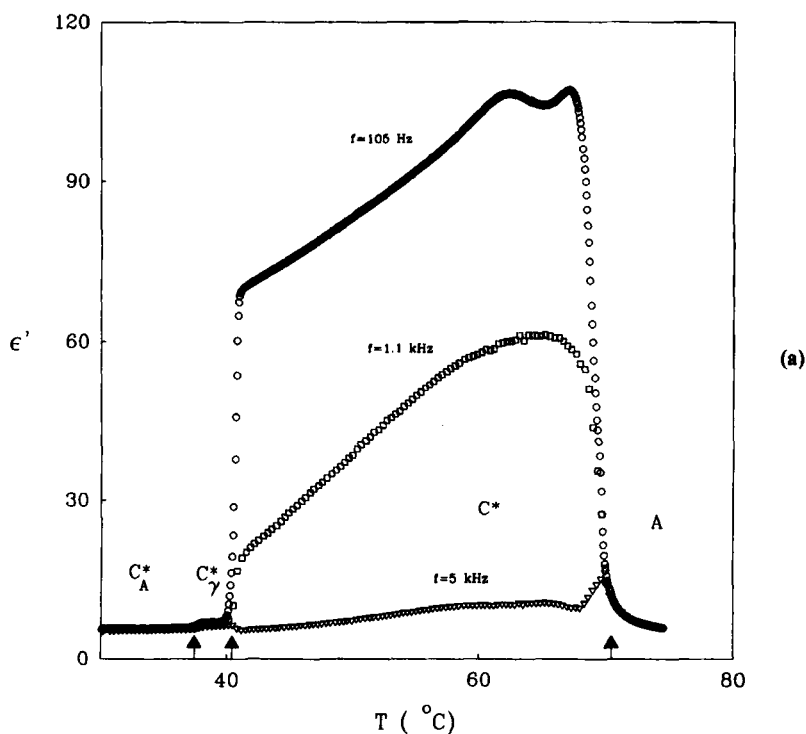


FIGURE 2

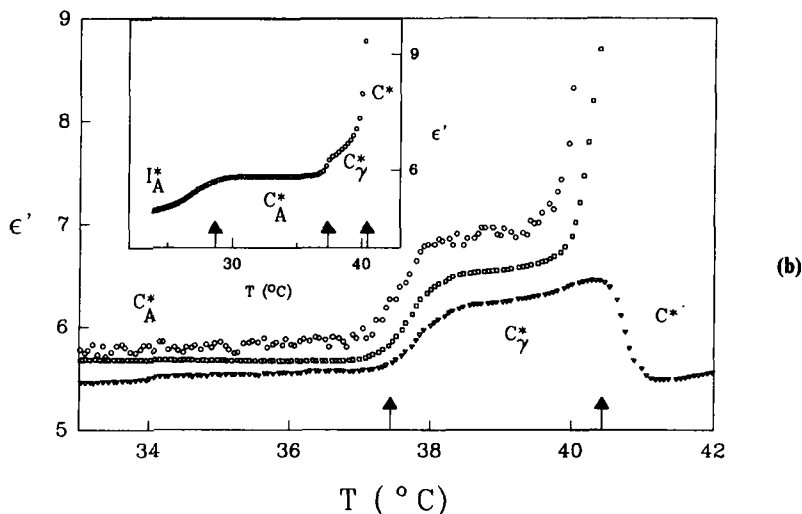


FIGURE 2 (a) Thermal variation of the real part of the transverse dielectric constant ϵ' at three different frequencies obtained using $50\mu\text{m}$ samples. For the sake of clarity, only every fifth point has been plotted for the 1.1 kHz and 5 kHz data sets. (b) data near the $C^* - C_\gamma^*$ and $C_\gamma^* - C_A^*$ transitions on an enlarged scale. The inset in (b) shows measurements near the $C_A^* - I_A^*$ transition, obtained with $9\mu\text{m}$ samples. The arrows indicate transition temperatures determined by DSC.

measurements. This temperature corresponds to the $C^* - C_\gamma^*$ transition. In fact, the change is much sharper in the high frequency data (see Fig. 2b) and is therefore useful in locating the $C^* - C_\gamma^*$ transition point. Finally, the $C_\gamma^* - C_A^*$ transition is accompanied by a small but noticeable reduction in the ϵ' values. These results can be seen as due to the influence of the Goldstone mode (recalling that the sample is quite thick). The contribution of this mode is large in the C^* phase, decreases in the C_γ^* phase and vanishes in the C_A^* phase.

We have already noted that with $50\mu\text{m}$ samples, measurements were not possible in the I_A^* phase due to the crystallisation of the material. This was overcome by using a thinner sample ($9\mu\text{m}$). The dielectric data in the I_A^* phase so obtained are shown in the inset of Figure 2b. The smooth variation across the $C_A^* - I_A^*$ transition is perhaps indicative of a continuous evolution from one phase to another and confirms that I_A^* is antiferroelectric.

The temperature dependence of the relaxation frequency f_R and dielectric strength $\Delta\epsilon$ obtained from dispersion measurements are shown in Figures 3 and 4. In the A phase, the relaxation is due to the soft mode. It is known that in the A phase, on approaching the $A - C^*$ transition, the relaxation frequency of the soft mode decreases while its dielectric strength increases. In the C^* phase the dominant contribution is due to the Goldstone mode

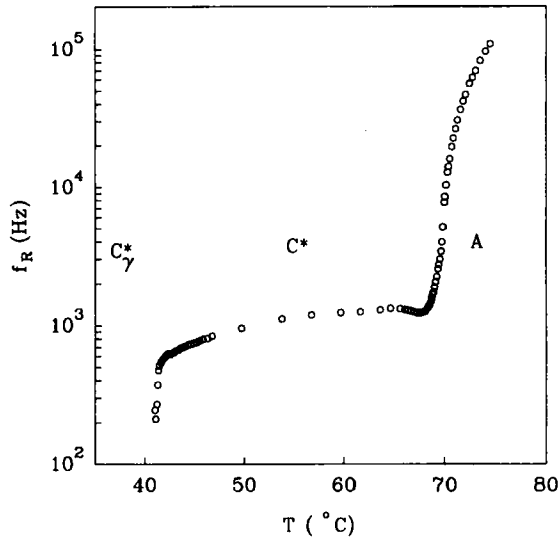


FIGURE 3 Plot of the dielectric relaxation frequency versus temperature.

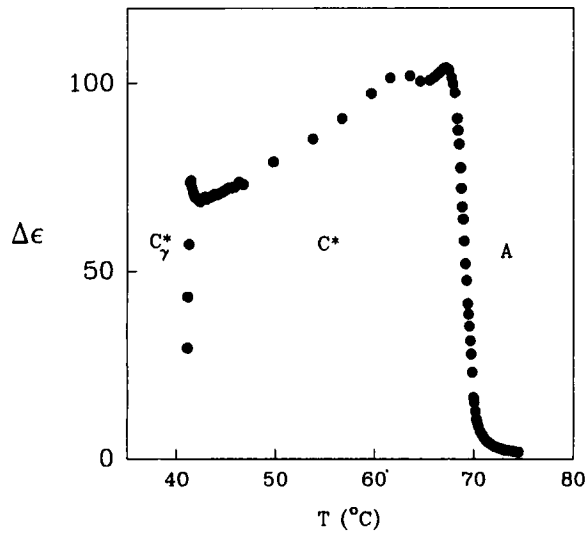


FIGURE 4 Dependence of the dielectric relaxation strength on temperature.

which masks the soft mode. The temperature dependence of the Goldstone mode relaxation frequency and the dielectric strength are primarily controlled by the thermal variation of the helical pitch. Experiments have shown that the value of the helical pitch is weakly dependent on temperature in the

C^* phase away from the $A - C^*$ transition, but drops abruptly close to it. Consequently the Goldstone parameters should show a strong temperature dependence in the vicinity of the $A - C^*$ transition, a fact which is confirmed in the f_R and $\Delta\epsilon$ data shown in Figures 3 and 4. Near the $C^* - C_\gamma^*$ transition, there is a large decrease in f_R and a small increase in $\Delta\epsilon$ followed by a sharp fall. A similar behaviour has been observed in earlier measurements [7]. In a recent paper, Hiller *et al.* [8] argue that the three-layer-block picture of C_γ^* phase could lead to a 3-fold increase in the helical pitch across the $C^* - C_\gamma^*$ transition. In such a case, the relaxation frequency which is inversely proportional to square of the helical pitch should decrease by about an order of magnitude on going from the C^* to the C_γ^* phase, in broad agreement with our data.

It has been shown by Isozaki *et al.* [9] that in these systems the application of a DC field leads to a variety of temperature-electric field (T-E) phase diagrams. Their data were obtained through electro-optic tilt angle or conoscopic observations. As we could observe very clear signatures of different transitions in our dielectric measurements, we could readily map such phase diagrams accurately from the dielectric data. As mentioned earlier, the changes observed are much sharper when the probing frequency is high. Therefore we used the 5 kHz data to map the T-E phase diagram. The results are shown in Figure 5. Both the $C^* - C_\gamma^*$ and $C_\gamma^* - C_A^*$ boundaries

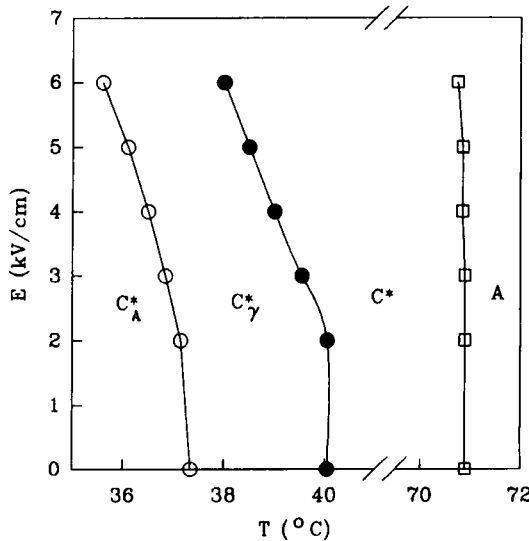


FIGURE 5 Temperature-electric field phase diagrams on the application of a DC bias field determined from dielectric measurements. The features bear good similarity to the ones obtained by the tilt angle/conoscopy method by Isozaki *et al.* [9].

have a negative slope while the $A - C^*$ transition temperature is only very weakly dependent on the applied electric field. The present phase diagram is similar to the ones obtained on different materials using the tilt angle/conoscopy method.

PRESSURE STUDIES

Recently we have carried out a series of high pressure measurements aimed at mapping out the pressure-temperature (P-T) phase diagrams as also studying the effect of pressure on the electrical properties [10]. All these studies have been in the ferroelectric C^* phase and near the $A - C^*$ transition. We have now investigated, to our knowledge the first time, the influence of pressure on the ferri- and antiferroelectric phases. The P-T diagram is shown in Figure 6a. As commonly observed, the transition temperatures of both the Isotropic-A and $A - C^*$ boundaries increase with increasing pressure, the slopes being $dT/dP = 31.3^\circ\text{C/kbar}$ and 25°C/kbar respectively. The $C_A^* - I_A^*$ boundary also shows a positive slope with $dT/dP = 16.3^\circ\text{C/kbar}$. The $C^* - C_\gamma^*$ and $C_\gamma^* - C_A^*$ transition boundaries show more interesting results. At lower pressures their transition temperatures increase with increasing pressure, but around 2.5 kbar there is a reversal in the trend (see enlarged plot in Fig. 6b). The phase boundaries curl towards the $C_\gamma^* - C_A^*$ line so that the C_γ^* and C_A^* phases get bounded resulting in two *three-phase* meeting points, namely, $C_\gamma^* - C_A^* - I_A^*$ point at ~ 3.05 kbar and $C^* - C_\gamma^* - I_A^*$ point at ~ 3.2 kbar. Notice that while the boundaries associated with the transition to the I_A^* phase go through the meeting points without any change in the slope, the $C^* - C_\gamma^*$ and $C_\gamma^* - C_A^*$ lines approach the respective meeting points at a finite angle. This feature, in fact, satisfies the topological requirement for a critical end point (CEP). The other "thermodynamic" condition to note is that at CEP the two boundaries which go through the meeting point without any slope change would be first-order in character while the other line must be second order. In the present case symmetry rules permit both the $C^* - C_\gamma^*$ and $C_\gamma^* - C_A^*$ transitions to be second order [11], but the $C_A^* - I_A^*$ transition, like the $C^* - I^*$ transition, can only be first order. These arguments suggest that the two meeting points may be critical end points. Detailed studies in the vicinity of the points should confirm this.

Another noteworthy feature observed in the phase diagram is the phenomenon of reentrance. In Figure 6b it is seen that at constant temperature, say $\sim 80^\circ\text{C}$, a sequence $C_\gamma^* - C_A^* - C_\gamma^*$ is observed as the pressure is varied

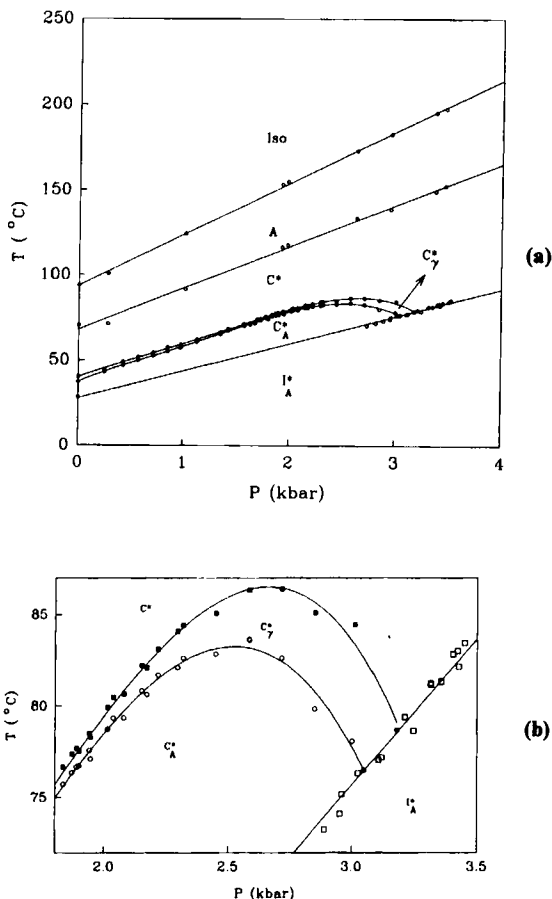


FIGURE 6 (a) Pressure-temperature phase diagram mapped using an optical transmission set up. While the $Iso-A$, $A - C^*$ and $C_A^* - I_A^*$ boundaries have a positive slope throughout, the $C^* - C_{\gamma}^*$ and $C_{\gamma}^* - C_A^*$ lines show a negative curvature at higher pressures. This results in the C_A^* and C_{γ}^* phases getting bound, leading to $C^* - C_{\gamma}^* - I_A^*$ and $C_{\gamma}^* - C_A^* - I_A^*$ meeting points. The data near the two meeting points are shown on an enlarged scale in (b). The topologies near the meeting points are consistent with the critical end point topology. The phase diagram also brings out reentrant behavior of the C^* and C_{γ}^* phases as the pressure is varied at constant temperature.

i.e., C_{γ}^* reenters. It may be mentioned that a reentrant C_{γ}^* phase has in fact been reported in the temperature-electric field phase diagram at room pressure for another compound [12]. Similarly it can be seen that the C^* phase reenters with varying pressure at constant temperature. We are planning to carry out pressure studies on a material having larger temperature range of the C_{γ}^* phase, which we believe may show a thermally-induced reentrant C_{γ}^* phase.

References

- [1] See e.g., A. Fukuda, Y. Takanishi, T. Isozaki, K. Ishikawa and H. Takezoe, *J. Mater. Chem.*, **4**, 997 (1994).
- [2] V. Faye, J. C. Rouillon, C. Destrade and H. T. Nguyen, *Liquid Crystals*, **19**, 47 (1995).
- [3] S. Krishna Prasad, R. Shashidhar, B. R. Ratna, B. K. Sadashiva, G. Heppke and S. Pfeiffer, *Liq. Cryst.*, **2**, 111 (1987).
- [4] A. N. Kalkura, R. Shashidhar and N. Subramanya Raj Urs, *J. Physique*, **44**, 51 (1983).
- [5] A. Ikeda, Y. Takanishi, H. Takezoe, A. Fukuda, S. Inui, S. Kawano, M. Saito and H. Iwane, *Jpn. J. Appl. Phys.*, **30**, L1032 (1991).
- [6] M. Neundorf, Y. Takanishi, A. Fukuda, S. Saito, K. Murashiro, T. Inukai and D. Demus, *J. Mater. Chem.*, **5**, 2221 (1995).
- [7] M. Glogarova, H. Sverenyak, H. T. Nguyen and C. Destrade, *Ferroelectrics*, **147**, 43 (1993).
- [8] S. Hiller, S. A. Pikin, W. Haase, J. W. Goodby and I. Nishiyama, *Jpn. J. Appl. Phys.*, **33**, L1096 (1994).
- [9] T. Isozaki, T. Fujikawa, H. Takezoe, A. Fukuda, T. Hagiwara, Y. Suzuki and I. Kawanura, *Phys. Rev. B.*, **48**, 13439 (1993).
- [10] S. Krishna Prasad, S. M. Khened and S. Chandrasekhar, *Ferroelectrics*, **147**, 351 (1993).
- [11] V. L. Lorman, A. A. Bulbitch, and P. Taledano, *Phys. Rev.*, **E49**, 1367 (1994).
- [12] H. Moritake, M. Ozaki, H. Taniguchi, K. Satoh and K. Yoshino, *Jpn. J. Appl. Phys.*, **33**, 5503 (1994).